Biosensors and Bioelectronics 65 (2015) 183–190

Contents lists available at ScienceDirect

Biosensors and Bioelectronics

journal homepage: www.elsevier.com/locate/bios

Gold nanocluster-based fluorescence biosensor for targeted imaging in cancer cells and ratiometric determination of intracellular pH

Changqin Ding [a], Yang Tian [a,b,*]

[a] Department of Chemistry, Tongji University, Siping Road 1239, Shanghai 200092, People's Republic of China
[b] Department of Chemistry, East China Normal University, North Zhongshan Road 3663, Shanghai 200062, People's Republic of China

ARTICLE INFO

Article history:
Received 25 July 2014
Received in revised form
30 September 2014
Accepted 13 October 2014
Available online 18 October 2014

Keywords:
Au nanoclusters
Ratiometric fluorescence biosensor
pH determination
Targeted imaging
Cancer cells
Folate receptor

ABSTRACT

The dysregulated pH is working as a mark of cancer. It is a challenge for developing a biosensor for targeted imaging in cancer cells and monitoring of intracellular pH. Here, a ratiometric fluorescence biosensor for pH determination was developed with targeted imaging into folate acceptor (FR)-rich cancer cells at the same time. AuNCs protected by bovine serum albumin (BSA) worked as reference fluorophore and fluorescein-isothiocyanate (FITC) acted as the response signal for pH. For targeted imaging of cancer cells, the AuNCs were simultaneously conjugated with folic acid (FA). The developed ratiometric biosensor can monitor pH with a wide linear range from 6.0–7.8 with a pKa at 6.84. Under every different pH condition, the probe showed high selectivity over various metal ions and amino acids with its fluorescence ratio stayed almost constant ($<5\%$). It also showed good cyclic accuracy when pH switched between 6.0 and 8.0, as well as low cytotoxicity. The AuNC-based inorganic–organic nanohybrid biosensor showed good cell-permeability, low cytotoxicity, and long-term photostability. Accordingly, the pH biosensor was employed to gain targeted imaging in FR^{+ve} Hela cells with FR^{-ve} lung carcinoma cells A549 as comparison, and achieved to monitor the pH changes in Hela cells.

1. Introduction

Intracellular pH (pHi) plays a critical role in the physiological and pathological processes (Roos and Boron, 1981). The regulation of pHi is essential for most cellular processes, including receptor-mediated signal transduction, calcium regulation, ion transport, cell volume regulation, vesicle trafficking, cellular metabolism, cell membrane polarity and so on (Golovina and Blaustein, 1997; Loiselle and Casey, 2003). Abnormal pHi shows great relationship with human physiology and pathophysiology diseases such as cancer, Alzheimer's disease, and cardiopulmonary problems (Izumi et al., 2003; Lagadic-Gossmann et al., 1999; Tang et al., 2007). Recent years, the detection of pHi value in cancer cells draws more attention, as the dysregulated pH is working as a mark of cancer (Zhang et al., 2010). It has been reported that the intracellular pH is higher than extracellular pH in cancers tumor, which may help to promote the proliferation, migration, invasion of cancer tumors and some other cancer processions (Webb et al., 2011). On this point, monitoring pH changes in cancer cells is critically important for studying cellular functions and gaining a better understanding of physiological processes.

Up to now, pH sensitive microelectrodes, nuclear magnetic resonance, UV–vis absorption spectroscopy, and fluorescence spectroscopy have been reported for the detection of pH *in vivo* (Zhang et al., 2010). Among these, fluorescence probe provides a powerful tool to assess pH *in vivo* and *in vitro* with technical and practical advantages such as high sensitivity, subcellular resolution and easy operation (Li et al., 2014; Patterson et al., 1997). In our previous work, a two-photon "turn-on" fluorescence probe has been designed based on carbon dots for monitoring pH changes in live cells and tissues (Kong et al., 2012). Unfortunately, this kind of "turn-on" fluorescence probe, as well as those reported "turn-off" fluorescent probes for pH remains two limitations: one is lack of accuracy in quantitative determination, because the fluorescence intensity changes with the variation of pH and the fluorescent probe unevenly distributes in live cells; another is their lack selectivity in recognition of different cells, because they could be took up by various kinds of cells without specific recognition. To solve these two problems, we designed a ratiometric fluorescent biosensor with targeted marker for imaging and biosensing of pH in cancer cells. Ratiometric fluorescence measurements can eliminate the influence of variations in the local probe concentration and distribution, thus enhancing the accuracy of measurements (Du et al., 2013; Fu et al., 2013; Gao et al., 2014; Miao et al., 2013;

* Corresponding author at: Department of Chemistry, Tongji University, Siping Road 1239, Shanghai 200092, People's Republic of China. Fax: +86 21 62237105.
E-mail address: ytian@chem.ecnu.edu.cn (Y. Tian).

http://dx.doi.org/10.1016/j.bios.2014.10.034
0956-5663/

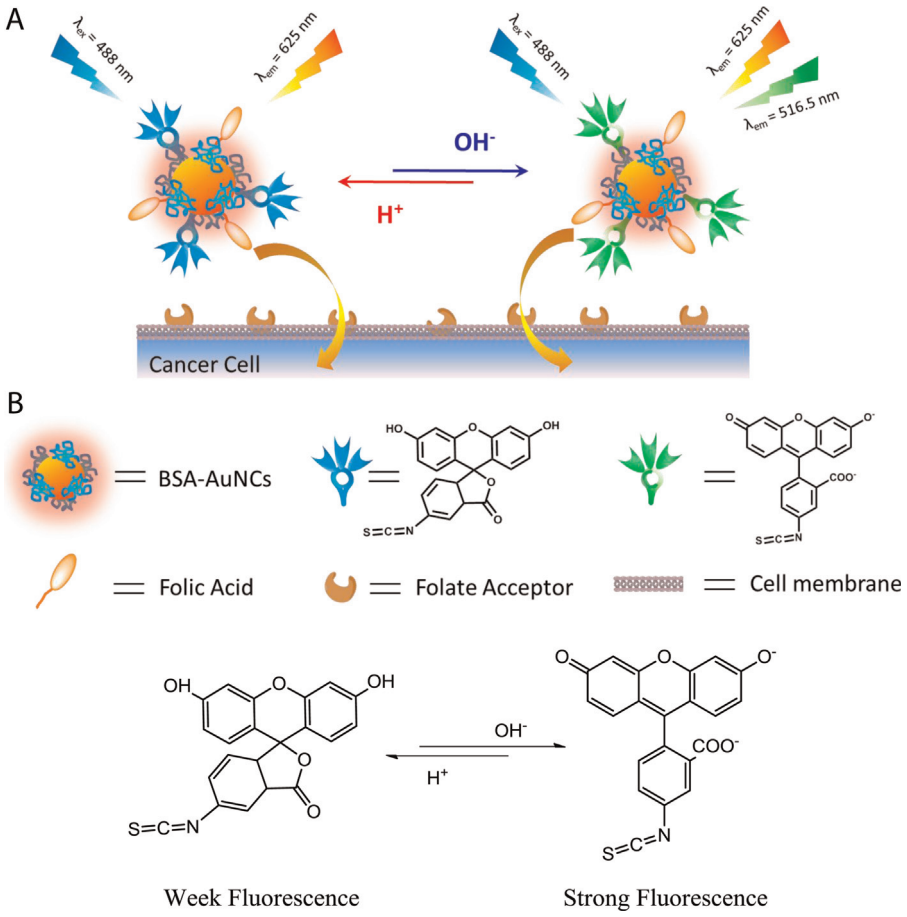

Fig. 1. (A) Working principle of the developed FA-FITC@AuNC fluorescent bisensor for pH detection and cancer cell-targeted imaging and (B) Reaction scheme of FITC with H^+ and OH^-.

Zhu et al., 2012). Silica nanoparticals and polymer gel coating with different dyes and quantum dots (QDs) were widely used as the reference fluorescences for construction of raiometric fluorescence probes (Dennis et al., 2012; Peng et al., 2010; Tsou et al., 2014). But these probes are difficult to enter into live cells because of their big sizes and some of them have high potential toxicity due to their heavy metal components. More recently, AuNCs have been reported as new type of luminescent nanomaterials for catalysis, sensors, and bioimaging because of their good biocompatibility, high electrocatalytic activity, and unique optical property (Kong et al., 2011; Liu et al., 2014; Sperling et al., 2008; Xie et al., 2009; Xue et al., 2012; Zhuang et al., 2014). AuNCs protected by BSA showed good photoluminescence properties with a large Stokes shift (~150 nm), good biocompatibility, and low cytotoxicity due to its small size (central core <5 nm) and BSA shell.

In this article, we developed a AuNC-based fluorescence biosensor for targeted imaging of cancer cells and ratiometric fluorescence detection of intracellular pH simultaneously. As shown in Fig. 1A, BSA-protected AuNCs were employed as reference signal and conjugated with FITC to form a ratiometric fluorescence probe FITC@AuNC for pH detection. Here, FITC acted as the specific recognition element for H^+ with fluorescence emission centered at 516.5 nm. When pH increases (OH^- increases), the lactone ring of FITC molecular will open to form anion, causing strong fluorescence emission; when pH decreased (H^+ increases), the lactone ring will closed with weak fluorescence (Fig. 1B), while the red fluorescence ascribed to AuNCs at 625 nm remained constant. On the other hand, FA was also hybrid on FITC@AuNC surface to form FA-FITC@AuNC fluorescent probe for targeted imaging of cancer cells. FA transports physiologically across the plasma membrane by using either reduced folate carrier or FR. The latter is frequently overexpressed in cancer cells, enabling FA be used as a good target-receptor for FR^{+ve} cancer cells (Lu and Low, 2002; Wang et al., 2013). The FA-FITC@AuNC biosensor can monitor pH gradients in a pH range of 6.0–7.8 with high selectivity, good sensitivity, and high cyclic accuracy. Meanwhile, AuNC-based fluorescent biosensor showed low-cytotoxicity and long-term stability against light illumination. Moreover, it also exhibited the ability to achieve target-imaging of FR^{+ve} cancer, indicating an acidification process and its recovery when these nanoparticles entering into cancer cells.

2. Material and methods

2.1. Reagents and chemicals

Gold (III) chloride trihydrate ($HAuCl_4 \cdot 3H_2O$, 99%), dimethyl sulfoxide (DMSO), nhydroxysuccinimide (NHS), and methyl thiazolyl tetrazolium (MTT) were purchased from Sigma-Aldrich. Fluorescein-isothiocyanate (FITC), N, N′-Dicyclohexylcarbodiimide (DCC), folic acid (FA), and ouabain octahydrate were obtained from Aladdin Chemistry Co. Ltd. Metal salts, bovine serum albumin (BSA), amino acids, glucose, diethylether, and triethylamine were obtained from Sinopharm Chemical Reagent Co. Ltd. Solutions of metal ions were all prepared from their chloride salts. Dialysis tube (MWCO: 3500) and Sephadex G50 were obtained from Ebioeasy Corporation and Biosharp Corporation separately. Cell culture media and supplements were supplied by Invitrogen Corporation. All chemicals from commercial sources were used as

received without further purification. All aqueous solutions were prepared with Milli-Q water (18.2 MΩ cm^{-1}).

2.2. Synthesis of AuNCs, FITC@AuNC, and FA-FITC@AuNC probes

BSA-stabilized AuNCs were synthesized according to a green bio-mineralization method (Xie et al., 2009) with a little modulation. The combination of FITC and AuNCs was achieved through the reaction between the isothiocyanate group of FITC and the amino group on the surface of AuNCs to form FITC@AuNC and stored at 4 °C. For preparation of FA-FITC@AuNC probe, AuNCs were firstly conjugated with FA by using coupling reagents DCC and NHS (Lee and Low, 1994). In a typical experiment, FA was reacted overnight with 500 mg DCC and 300 mg NHS at room temperature. After filtration, the reaction product FA@AuNC was precipitated and washed three times with diethylether, dried under vacuum, and stored as yellow powder. Then FA@AuNC solution was mixed with the solution of NHS-folate in DMSO with appropriate proportion in dark for another 2 h. Followed, FITC in EtOH was added and the reactant was stirred in dark at room temperature for another 12 h. Finally, the nanohybrid probe was dialyzed in PBS (0.05 M, pH=7.4) for 8 h by using dialysis tube, purified through Sephadex G50 column and stored at 4 °C.

3. Results and discussion

3.1. Characterization of AuNCs and FA-FITC@AuNC

The as-prepared AuNCs showed mono-dispersed with average size of ~5 nm, as shown in Fig. 2A. A further observation revealed that the AuNC was consistent with ⟨111⟩ spacing of Au (Fig. 1B), which was confirmed by XRD data with a diffraction peak at 38.56° (JCPSD no. 04-0784, Fig. 2B). After combined with FA and FITC, such diffraction peak shifted to 35.32°, indicating the increase of Au lattice from ~2.06 Å to ~2.24 Å. The change was also evident by XPS results. As demonstrated in Fig. 2C, the Au 4f XPS spectrum of AuNCs displayed a dominant component of Au°: 83.5 eV (Au $4f_{7/2}$) and 87.3 eV (Au $4f_{5/2}$), while Au 4f XPS spectrum of FA-FITC@AuNC showed two main peaks at 84.1 eV (Au $4f_{7/2}$) and 87.7 eV (Au $4f_{5/2}$), typically ascribed to Au^{+} (Guével et al., 2011; Wei et al., 2010). FT-IR spectrum of AuNCs (Fig. 2D, curve a) exhibited four characteristic peaks located at 3450 cm^{-1} (V_{O-H}), 1260 cm^{-1} (V_{C-H}), 1662 cm^{-1} ($V_{C=O}$), and 1540 cm^{-1} (V_{N-H}). The presence of these hydrophilic groups including $-NH_2$, –COOH and/or –OH imparts AuNCs water-solubility. On the other hand, FT-IR spectrum for FITC (Fig. 2D, curve b) shows four characteristic peaks located at 3420 cm^{-1}, 2040 cm^{-1}, 1620 cm^{-1}, and

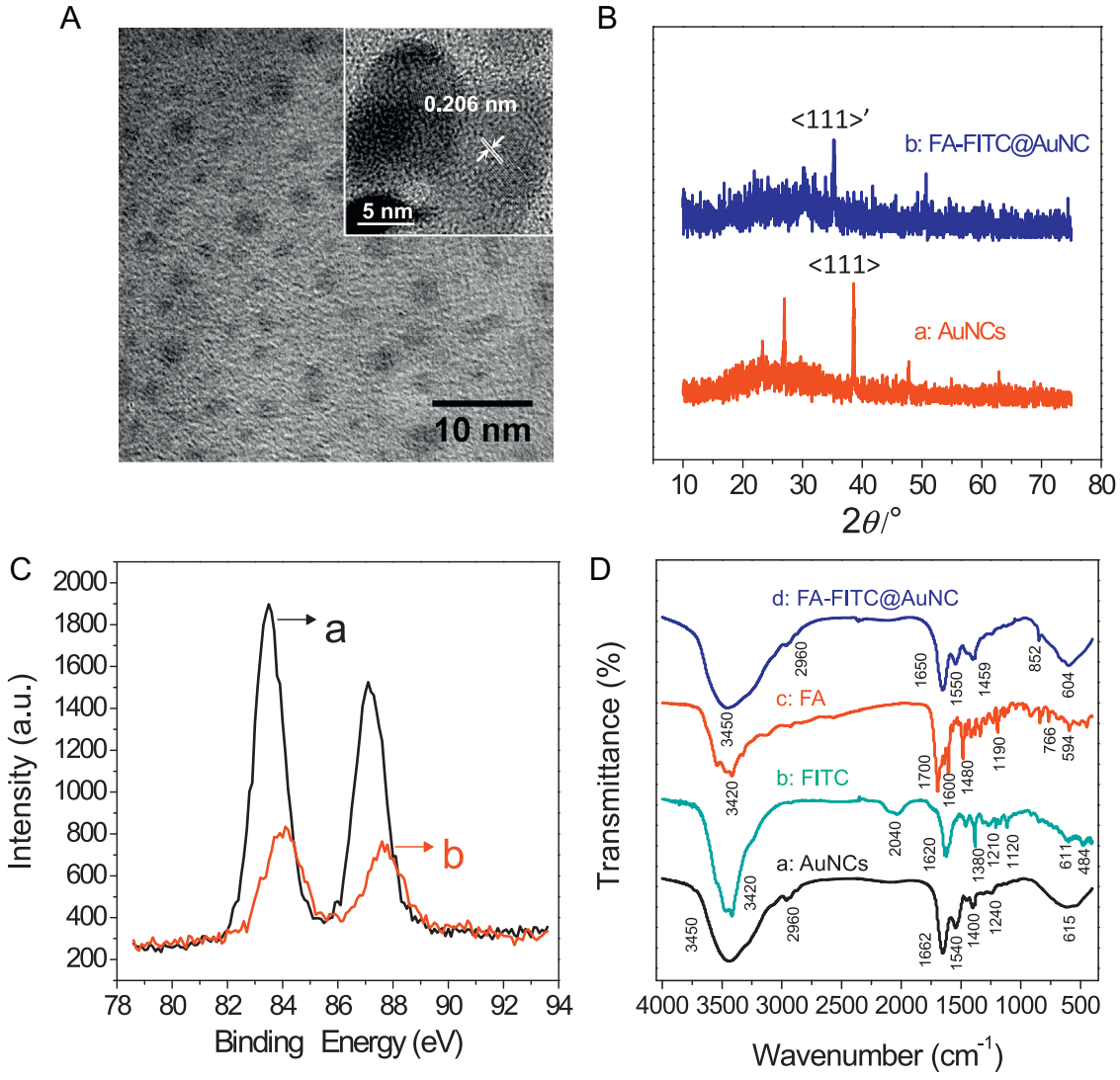

Fig. 2. Characterization of the fluorescent biosensor. (A) TEM and HRTEM (inset) images of AuNCs; (B) X-ray diffraction patterns of (a) AuNCs and (b) FA-FITC@AuNC; (C) XPS data of (a) AuNCs and (b) FA-FITC@AuNC; (D) FT-IR spectra of (a) AuNCs, (b) FITC, (c) FA and (d) FA-FITC@AuNC.

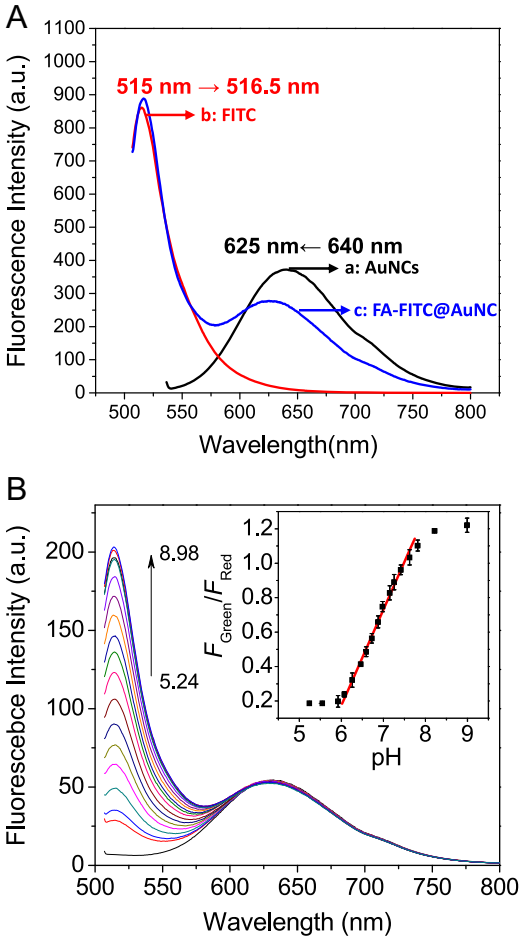

Fig. 3. Fluorescent determination of pH. (A) Fluorescence spectra of (a) AuNCs, (b) FITC, and (c) FA-FITC@AuNC under 488 nm excitation; (B) Fluorescence spectra of the ratiometric biosensor to various pH titration. Inset: Plot of F_{Green}/F_{Red} as a function of the pH (5.0–9.0) (excited at 488 nm, F_{Green}: 510–550 nm, F_{Red}: 580–680 nm).

1380 cm^{-1}, which are ascribed to the vibration of O–H, N═C═S, C═O and C–O–C respectively. Meanwhile, five peaks located at 3420 cm^{-1}, 1700 cm^{-1}, 1600 cm^{-1}, 1480 cm^{-1}, and 1190 cm^{-1} were clearly observed for FT-IR spectrum of FA, corresponding to the vibration of V_{O-H}, $V_{C=O}$, δ_{N-H}, V_{C-N} and V_{C-O} respectively. After FITC and FA were conjugated on AuNCs surface, the appeared peaks at 1650 cm^{-1} (Amide I $V_{C=O}$) and 1459 cm^{-1} (Amide III V_{C-N}), and the disappeared peak at 2040 cm^{-1} ($V_{N=C=S}$) in the IR spectra (Fig. 2D, curve d) indicated the successful attachment of FA and FITC on AuNCs by covalent combining with BSA.

The fluorescence emission of AuNCs was observed to be centered at 640 nm under excitation at 488 nm, as shown in Fig. 3A (curve a). Using rhodamine B as a standard, the fluorescence quantum yield (QY) of AuNCs was estimated to be ~9% (Fig. S1, Supplementary Information (SI)). However, after combined with FITC and FA, such emission shifted to 625 nm. Meanwhile, the emission peak of FITC shifted from 515 nm to 516.5 nm upon excitation of 488 nm (Fig. 3A, curve b). The successful preparation of FA-FITC@AuNC was also proved by UV–Vis spectrum when the as-prepared probe was purified through Sephadex G50 column, in which FA-FITC@AuNC flowed out firstly (Fig. S2A, I, SI) and then FA-FITC–BSA followed (Fig. S2A, II, SI). The chromatogram was obtained by detecting the intensity of fluorescence emission (λ_{ex} =488 nm) and UV–Vis absorbance at the same time. The intensities of fluorescent emissions at 516.5 nm and 625 nm presented the existences of FITC and AuNCs, respectively. UV–Vis absorption peaks at 280 nm and 350 nm indicated the combination of BSA and FA (Stella et al., 2000). Furthermore, UV–Vis absorption spectrum showed a new absorption shoulder around 355 nm after the combination of FA (Fig. S2B, *SI*), which also indicates the successful conjugation of FA, FITC and AuNCs.

3.2. Analytical performance of FA-FITC@AuNC biosensor for pH determination

The standard fluorescence pH titration was performed in PBS at the excitation of 488 nm, as shown in Fig. 3B. In this ratiometric biosensor, the organic molecule FITC was used as response signal for determination of pH, while AuNC served as reference signal because of its good stability under different pH (Fig. S3, SI). With the increasing pH of the buffer solution, the green emission from FITC continuously increased, while the red fluorescence ascribed to AuNCs stayed constant. As a result, F_{Green}/F_{Red}, the ratio of the integrated intensities at 510–550 nm (F_{Green}) and 580–680 nm (F_{Red}), gradually increased with the increasing pH. The signal ratio showed good linearity with pH in the range of 6.0–7.8 with a pKa at 6.84, as plotted in the inset of Fig. 3B. As the 2δ of the pH titration experiments is 0.099, suggesting that the FA-FITC@AuNC could detect pH change with a level of ~0.1.

Much importantly, the complexity of intracellular system presents a great challenge for biosensors in requirement of selectivity and stability. The selectivity experiments were carried out by monitoring the F_{Green}/F_{Red} ratio of the fluorescent biosensor in the presence of metal ions and amino acids which may coexist in living system. Various metal ions such as aboundant cellular cations (1 mM for K^+, Na^+, Ca^{2+}, Mg^{2+}) and trace metal cations in organisms (10 μM for Co^{2+}, Cd^{2+}, Cu^{2+}, Fe^{2+}, Fe^{3+}, Mn^{2+}, Ni^{2+}, Zn^{2+}) were tested under three different pH conditions (pH 6.34, 7.25, and 8.09 respectively). As shown in Fig. 4A, under the same pH conditions, there is no obvious difference in the F_{Green}/F_{Red} ratio in the presence of various cations (< 5%) compared to that in different pH situations. Similarly, several typical amino acids and glucose (10 μM) were examined under three different pH conditions. It could be seen that the F_{Green}/F_{Red} ratio of fluorescent biosensor coexisted with various amino acids and glucose stayed nearly unchanged under the same pH condition, while shifted with the changes of pH (Fig. 4B). The results indicate the high selectivity of the developed ratiometric probe for determination of pH in the complicated live cells.

The photostability of FA-FITC@AuNC biosensor was also investigated under different pH conditions (pH 6.19, 7.42, and 8.06) and summarized in Fig. 4C. After being exposed to a fluorescence spectrophotometer (λ_{ex}=488 nm) equipped with a 90 W Xenon lamp for 2 h, no obvious changes (< 5%) were observed for the F_{Green}/F_{Red} ratio of the biosensor under every pH condition, suggesting the good photostability of this AuNC-based inorganic–organic fluorescent biosensor. Fig. 4D showed the good fluorescence reversibility responses of FA-FITC@AuNC biosensor in the ratio of integrated intensities (F_{Green}/F_{Red}) in a PBS solution when pH was switched between 6.0 and 8.0 for three cycles. Besides, the relationship between the fluorescence ratio (F_{Green}/F_{Red}) and reaction time showed that such probe could quickly response to pH changes within 30 s (Fig. S4, *SI*). These experiments indicated that the dual-emission FA-FITC@AuNC fluorescent probe had high selectivity, long-term stability, good reversibility and quick response for pH determination in biological system.

3.3. Cytotoxicity.

The possibility of FA-FITC@AuNC probe for molecular receptor-targeted optical detection of cancer was tested in three types of cancer cell lines with different levels of FR expression: FR^{+ve} Hela

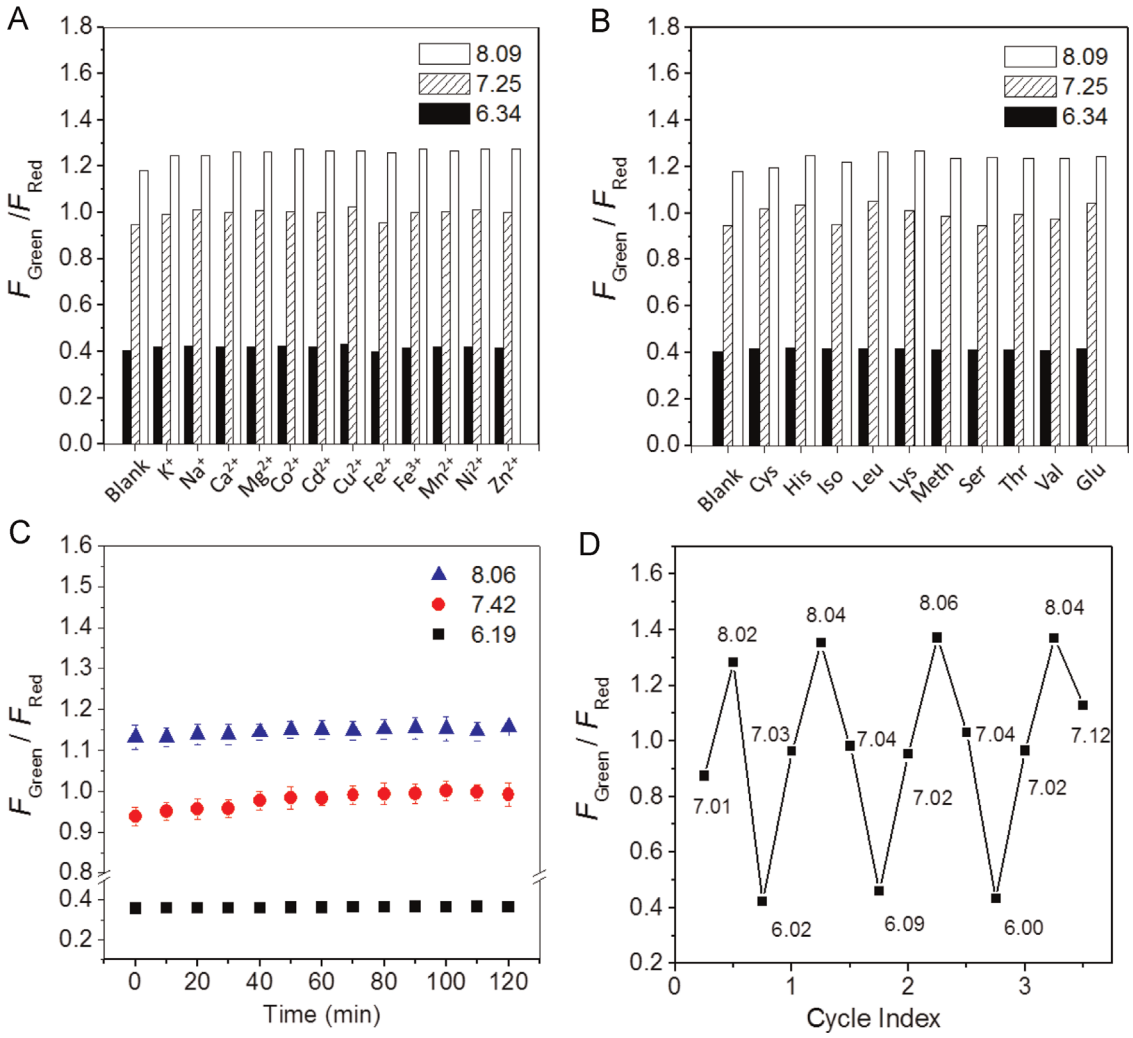

Fig. 4. Selectivity, photostability, and reproducibility test. (A and B) Fluorescence responses of FA-FITC@AuNC under different pH of 6.34, 7.25, and 8.09 respectively, (A) toward various metal ions (1 mM for Na^+, K^+, Ca^{2+}, and Mg^{2+}; 10 μM for other cations); and (B) toward various amino acids (10 μM for cysteine, valine, histidine, isoleucine, leucine, lysine, methionine, serine, threonine, and glutamic acid) and 10 μM glucose. (C) Photostability of FA-FITC@AuNC i under different pH of 6.19, 7.42, and 8.06 respectively for 2 h. Error bars represent standard error measurements (S.E.M.) of three parallel experiments. (D) Fluorescence reversibility responses of FA-FITC@AuNC between pH 6.0 and 8.0.

cells, FR^{-ve} lung carcinoma cells A549, and FR^{-ve} human kidney cells 293 T. To develop further biological imaging applications, the long-term cellular toxicity of both fluorescent probes were determined by standard MTT assays. In the presence of FITC@AuNC probes with concentration from 5 to 100 μg mL^{-1}, the cellular viabilities of Hela cells were estimated to be greater than 85% and 80% after incubation for 24 and 48 h (Fig. S5A, SI), while those of A549 cells were greater than 80% and 75% (Fig. S5B, *SI*). Meanwhile, the cellular viabilities of cells treated with FA-FITC@AuNC probes for 24 and 48 h were up to 80% and 75% in Hela cells, as well as 85% and 90% in A549 cells. Besides, non-cancer FR^{-ve} human kidney 293 T survived much more with FA-FITC@AuNC probe (> 88% for 24 h, > 93% for 48 h) than with FITC@AuNC probe (> 93% for 24 h, > 75% for 48 h) under the same treatment concentration (Fig. S5C, SI). These results indicated that both FITC@AuNC and FA-FITC@AuNC probes is generally low-toxic for cellular imaging, possibly because of good biocompatibility of the surrounded biomolecule BSA.

3.4. *FR-targeted imaging and cellular uptake of FA-FITC@AuNC*

The FR-targeted optical images of FA-FITC@AuNC and FITC@AuNC were obtained by using FR^{+ve} Hela cells and FR^{-ve} lung carcinoma cells A549. Fig. 5 presents the overlap images of fluorescent channel F_{Red} (580 nm–680 nm) and bright field of FR^{-ve} A549 cells and FR^{+ve} Hela cells, which were treated with FA-FITC@AuNC and FITC@AuNC. Hoechst 33342 staining was carried out to differentiate the nucleus from cytosol. It demonstrated that AuNCs probes were dispersed mainly near the nucleus of cells (Fig. S6, SI). The relative difference in the uptake of probes was measured by collecting the fluorescence of F_{Red} (Fig. 5C). There is no obvious difference between the consuming amount of FITC@AuNC probes into FR^{+ve} Hela cells (Fig. 5A1) and FR^{-ve} A549 cells (Fig. 5B1) after incubation of 2 h. It appeared to be no significant staining or cellular uptake responding to FA-mediated process in the intracellular uptake process of FITC@AuNC probes. However, FR^{+ve} Hela cells took nearly three times of FA-FITC@AuNC probes (Fig. 5A2) as much as of FITC@AuNC probes (Fig. 5A1). As compared, FR^{-ve} A549 cells and 239 T cells took up less FA-FITC@AuNC than Hela cells did during the same culture time (Fig. S8, SI), which was corresponded with the lack of folate receptor on its cytomembrane. Furthermore, when Hela cells were pretreated with FA for 2 h, the uptake of FA-FITC@AuNC into Hela cells significantly decreased (Fig. 5A3). These results clearly suggest that FA-FITC@AuNC were specifically taken up by Hela cells via a process corresponding to the FR on the surface of cells, and gathered near

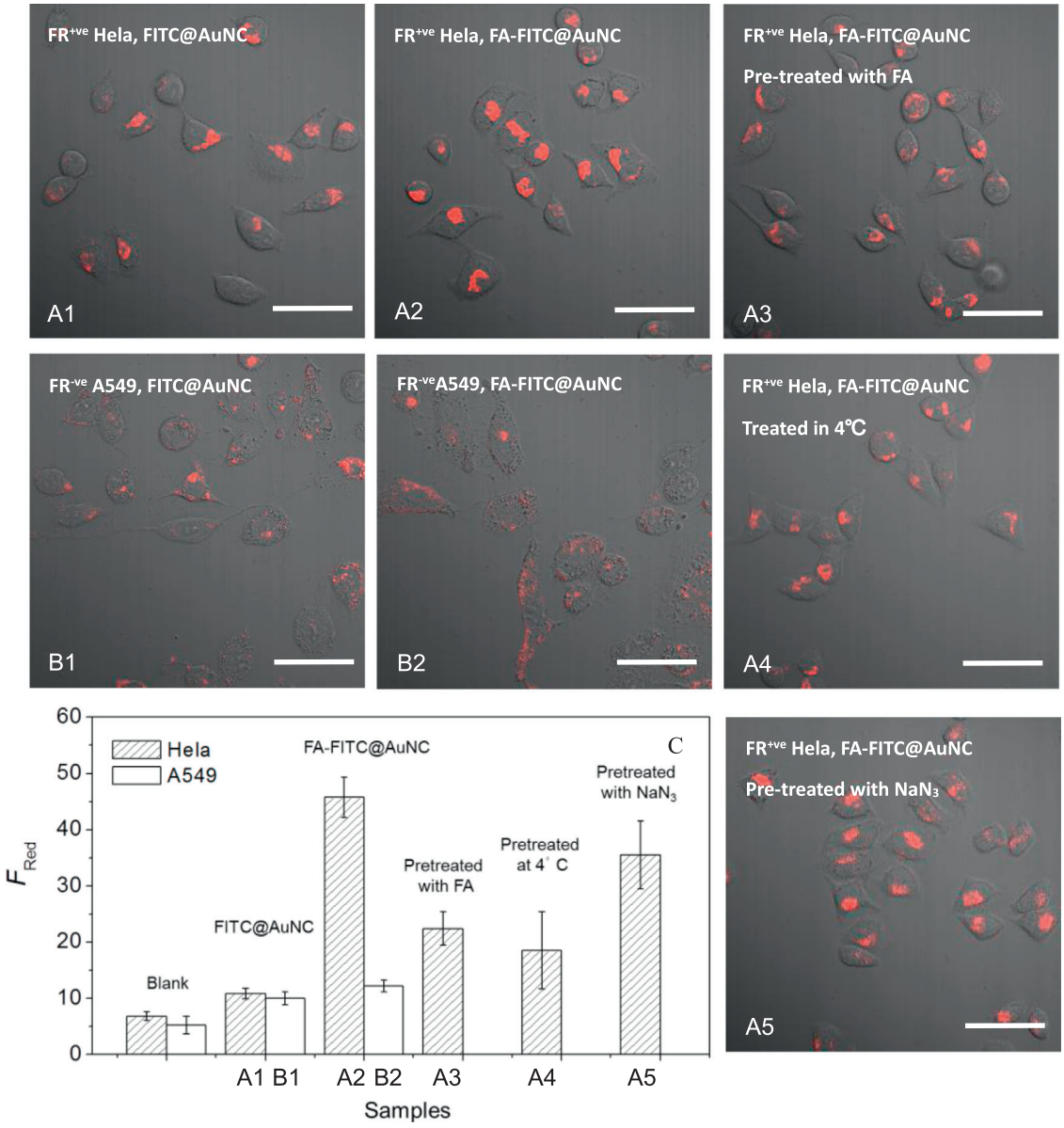

Fig. 5. Fluorescent microscopic images showing interaction of FA-FITC@AuNC and FITC@AuNC with (A) Hela cells and (B) A549 cells: (A1) FR^{+ve} Hela and (B1) FR^{-ve} A549 cells with FITC@AuNC, (A2) FR^{+ve} Hela and (B2) FR^{-ve} A549 with FA-FITC@AuNC of incubation for 2 h at 37 °C, and FR^{+ve} Hela cells incubated with FA-FITC@AuNC for 2 h after treated (A3) with FA for 2 h, (A4) at 4 °C, and (A5) 10 mM NaN_3 for 2 h. (C) Cellular internalization amount of FA-FITC@AuNC and FITC@AuNC in different types of cell lines under various treatments. Error bar: standard error measurements (S.E.M.). Scale bar: 50 μm.

nucleus with the fluorescence intensity remaining intact. When cells were cultured with probes at 4 °C (Fig. 5A4) or pretreated with NaN_3 (Fig. 5A5) for 2 h to block the energy-dependent endocytosis, the consuming amount of probes were identically decreased (Fig. 5C). These results indicate that the uptake of FA-FITC@AuNC probes were taken-up into Hela cells mainly via a pathway with folic-receptor involved and energy dependent. It also indicated the maintenance of the probes and its potential application for pH detection in the intracellular regions.

Next, the process of cellular uptake of FA-FITC@AuNC probes into Hela cells were monitored by culturing Hela cells in serum-free media with 50 μg mL^{-1} FA-FITC@AuNC probes at 37 °C for 0.5 h, 1 h, 2 h, 4 h, and 24 h, respectively. The fluorescence intensities from 510 to 550 nm (F_{Green}) and from 580 to 680 nm (F_{Red}) were collected to indicate pH values in the cellular uptake process as well as the consuming amount of probes in cells. Fig. S7 (SI) showed that after 2 h incubation, the consuming of probes into cells reached maximum. Then, the amount of probes in cells decreased rapidly and almost disappeared after 24 h incubation (Fig. S7A-E, SI). It indicates a quick metabolism as well as the low cytotoxicity of such probes in cells. Besides, it could be noticed that the probes were firstly gathered near cytomembrane (Fig. S7B, SI), then transferred near nuclear (Fig. S7D, SI). In this process, the emission of F_{Green} from FITC increased gradually with the color of the fluorescent merged images turned from false red (Fig. S7B, *SI*) to yellow (Fig. S7D, SI). It suggests that the pH of the environment of probes increased among the probe moving from near-cytomembrane to near-nuclear region.

Though the precise mechanism of FR transport of FA into cells remained unsolved, it is clear that folate conjugates were taken up nondestructively by mammalian cells via receptor-mediated endocytosis (Lu and Low, 2002; Rothberg et al., 1990a, 1990b; Turek et al., 1993). Such folate conjugates were observed to internalize endosomes after they bond to FR on the cancer cell surface (Turek et al., 1993; Varma and Mayor, 1998; Wu et al., 1997). It has also been reported that folate conjugate-containing endosomes have

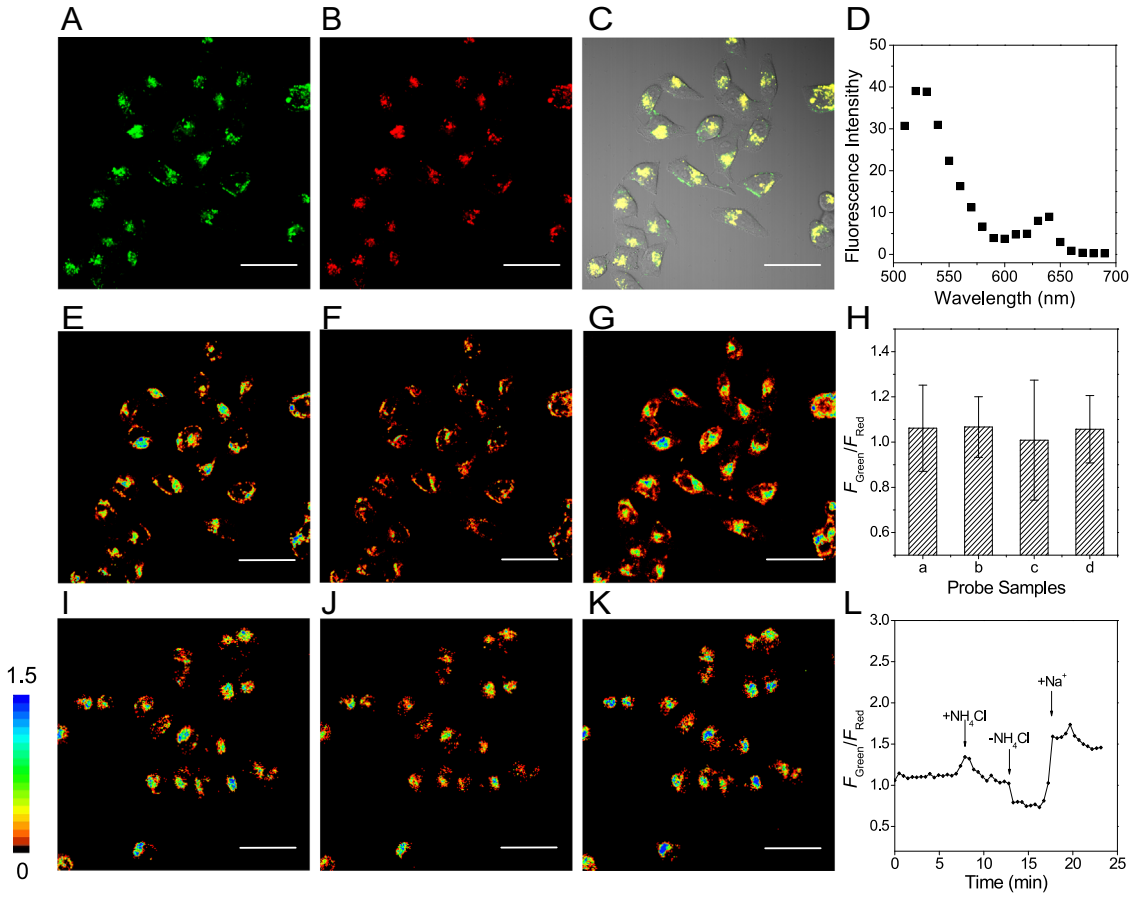

Fig. 6. (A–C) Confocal fluorescence images of (A) F_{Green} (510–550 nm), (B) F_{Red} (580–680 nm), and (C) overlapped fluorescence and bright field image of Hela cells incubated with FA-FITC@AuNC for 1 h excited by 488 nm; (D) Fluorescence emission scan from Hela cells with FA-FITC@AuNC probes. (E–G) Na^+–H^+ exchange dependent pseudo color images (F_{Green}/F_{Red}) of Hela cells with FA-FITC@AuNC probes stimulated by ouabain. (E) Hela cells incubated in Cl^--free Ringer's solutions containing 0.1 mM ouabain for 45 min, followed by (F) treated in Na^+-free Ringer's solutions for another 5 min, and (G) adding 100 mM Na^+ for another 5 min. (H) Bar graph representing F_{Green}/F_{Red}. (I–L) Na^+–H^+ exchange dependent pseudo color images (F_{Green}/F_{Red}) of Hela cells with FA-FITC@AuNC probes stimulated by NH_4Cl: (I) Hela cells are incubated in Cl^--containing Ringer's solutions with 30 mM NH_4Cl for $_4$ min, followed by (J) washing NH_4Cl from the solution, and (K) adding Na^+-containing Ringer's solutions for another 2 min; (L) Bar graph representing F_{Green}/F_{Red}. Values are the mean ratios generated from the intensities from five randomly selected fields. Error bars represent standard error measurements (S.E.M.). Scale bar: 50 μm.

been shown to have pH values between 4.3 and 6.9 due to a process called endosome acidification (Lee et al., 1996). As a targeted-introducer, FA acted a similar role in the uptake of FA-FITC@AuNC probe for the detection of intracellular pH. As a result, FA-FITC@AuNC probe entered FR^{+ve} Hela cells specifically via a pathway corresponding to its rich folate receptors on the surface. Such process was energy-depended, and could be blocked by low temperature or the presence of NaN_3. After being taken into the cells, the two emissions (F_{Green} and F_{Red}) of probe acted differently when it transferred from the regions near cytomembrane to gather near the nuclear. In this transmission, the average ratio of two emission channel increased gradually, indicating an increase in the pH of the intracellular environment.

3.5. Bioimaging and biosensing of pH in cancer cells

According to the fluorescence images (Fig. 6A and B) and their overlay images with bright-field image (Fig. 6C), it was clear that the probe had good cell-permeability. The fluorescence scan in Hela cells treated with FA-FITC@AuNC probes (Fig. 6D) confirmed the present probes maintained the dual-emission in cellular environment, with two emissions centered at 520 nm and 640 nm. The emissions in cells had a little red-shift compared to that in PBS due to the various cellular environment and deviations from different detectors (Zhuang et al., 2014).

Next, FA-FITC@AuNC biosensor was used in the application of intracellular pH detection. The Na^+–H^+ exchange has been a common mechanism for regulating cytosolic pH (Paradiso et al., 1984). Upon excitation at 488 nm, the ratio images of Hela cells treated with FA-FITC@AuNC were collected from two separated channels. By using a "pseudo color image" technology, the ratio value of the gray value of green channel and red channel was coded into different colors: red for the ratio of 0.1 and blue for the ratio of 1.5. After Hela cells were incubated in Cl^--free Ringer's solutions containing 0.1 mM ouabain for 45 min, the average emission ratio F_{Green}/F_{Red} is 1.061 ± 0.191 (Fig. 6E), similar to that in Hela cells incubated without ouabain treatment (Fig. 6H). Then, the ratio slightly decreased to 1.008 ± 0.265 when the cells were continuously incubated with a Na^+-free Ringer's solutions for another 5 min (Fig. 6H). The pseudo color clearly changed from blue to red (Fig. 6F). Such change indicated a rapidly acidification of cells under stimulate of the Na^+-free Ringer's solutions. After adding another 100 mM Na^+ solution, such ratio increased back to 1.057 ± 0.149 (Fig. 6G and 6 H), suggesting a recover of pH in the intracellular environment.

In another set, Hela cells with FA-FITC@AuNC were incubated in a Cl^--containing Ringer's solution for 30 min, then treated with 30 mM NH_4Cl for 4 min (Fig. 6I). The acid load was achieved by washing the NH_4Cl from the solutions (Fig. 6J). After another stimulate by Na^+, cells would come alkalinized to a higher pH, with

the pseudo-color image turned into blue (Fig. 6K). Such changes was monitored by using a mode of time scan (Fig. 6L). It could be noticed that after the remove of NH_4Cl, the ratio value of F_{Green} and F_{Red} channels decreased to 0.975 ± 0.040, indicate the pH in cells decreased to ~6.5. As the addition of Na^+, the ratio value of two channels increased to 1.622 ± 0.066 firstly, then recovered to 1.495 ± 0.059. It showed that such stimulate will cause a sudden increase of pH in cells, then recovered after ~4 min. These initial experiments in Hela cells demonstrated that FA-FITC@AuNC probe could be used to observe the changes of pH in live cells through the fluorescence ratio of different emission channels, suggesting the great potential of this dual-emission probe for further fundamental biology researches.

4. Conclusions

To conclude, a ratiometric fluorescence biosensor for pH detection, FA-FITC@AuNC, has been developed successfully for specific bioimaging and biosensing in cancer cells at the same time. In this self-calibration biosensor, fluorescent AuNCs work as reference signal, FITC plays the role for pH response and FA acts as specific recognition element for cancer cells target. The developed biosensor has been used to monitor pH gradients in a pH range of 6.0–7.8 with good sensitivity, high cyclic accuracy, and short response time. It also exhibits high selectivity over various metal ions and biological species. Furthermore, the AuNC-based inorganic-organic biosensor shows good biocompatibility and long-term stability against light illumination. As a result, the target imaging have been testified by using FR^{+ve} Hela cells, FR^{-ve} A549 cells and FR^{-ve} 293 T cells, and achieved the biosensing of pH in Hela cells. It has been also confirmed an acidification process and its recovery in the transversion of FA conjugates entering into cancer cells. This investigation has provided a methodology to designing the ratiometric fluorescent biosensor with targeted molecules, by conjugating different function units, such as targeted and detector molecules on one kind of specific nanomaterial. In addition, this work can be extended to construct future ratiometric fluorescent biosensors for targeted imaging, drug deliver, or the detection of other biomolecules, such as metal ions, proteins, and other biological species.

Acknowledgments

This work was financially supported by the NSFC (21175098, and 21175044) and National Nature Science Fund for distinguished young scholars (21325521).

Appendix A. Supplementary material

Supplementary data associated with this article can be found in the online version at doi: http://dx.doi.org/10.1016/j.bios.2014.10.034

References

Dennis, A.M., Rhee, W.J., Sotto, D., Dublin, S.N., Bao, G., 2012. ACS Nano 6, 2917–2924.
Du, F., Ming, Y., Zeng, F., Yu, C., Wu, S., 2013. Nanotechnology 24, 365101.
Fu, Y., Ding, C., Zhu, A., Deng, Z., Tian, Y., Jin, M., 2013. Anal. Chem. 85, 11936–11943.
Gao, X., Ding, C., Zhu, A., Tian, Y., 2014. Anal. Chem. 86, 7071–7078.
Golovina, V.A., Blaustein, M.P., 1997. Science 275, 1643–1648.
Guével, X.L., HÖtzer, B., Jung, G., Hollemeyer, K., Trouillet, V., Schneider, M., 2011. J. Phys. Chem. C 115, 10955–10963.
Izumi, H., Torigoe, T., Ishiguchi, H., Uramoto, H., Yoshida, Y., Tanabe, M., Ise, T., Murakami, T., Yoshida, T., Nomoto, M., Kohno, K., 2003. Cancer Treat. Rev. 29, 541–549.
Kong, B., Zhu, A., Ding, C., Zhao, X., Li, B., Tian, Y., 2012. Adv. Mater. 24, 5844–5848.
Kong, B., Zhu, A., Luo, Y., Tian, Y., Yu, Y., Shi, G., 2011. Angew. Chem. Int. Ed. 50, 1837–1840.
Lagadic-Gossmann, D., Rissel, M., Galisteo, M., Guillouzo, A.B., 1999. J. Pharmacol 128, 1673–1682.
Lee, R.J., Low, P.S., 1994. J. Biol. Chem. 269, 3198–3204.
Lee, R.J., Wang, S., Low, P.S., 1996. Biochim. Biophys. Acta 1312, 237–242.
Li, P., Xiao, H., Cheng, Y., Zhang, Wen, Huang, F., Zhang, W., Wang, H., Tang, B., 2014. Chem. Commun. 50, 7184–7187.
Liu, J., Guan, Z., Lv, Z., Jiang, X., Yang, S., Chen, A., 2014. Biosens. Bioelectron 52, 265–270.
Loiselle, F.B., Casey, J.R., 2003. Methods. Mol. Biol. 227, 259–280.
Lu, Y., Low, P.S., 2002. Adv. Drug. Deliv. Rev. 54, 675–693.
Miao, F., Song, G., Sun, Y., Liu, Y., Guo, F., Zhang, W., Tian, M., Yu, X., 2013. Biosens. Bioelectron 50, 42–49.
Paradiso, A.M., Tsien, R.Y., Machen, T.E., 1984. Proc. Natl. Acad. Sci. 81, 7436–7440.
Patterson, G.H., Knobel, S.M., Sharif, W.D., Kain, S.R., Piston, D.W., 1997. Biophys. J. 73, 2782–2790.
Peng, H., Stolwijk, J.A., Sun, L., Wegener, J., Wolfbeis, O.S., 2010. Angew. Chem. Int. Ed. 49, 4246–4249.
Roos, A., Boron, W.F., 1981. Physiol. Rev. 61 (2), 296–434.
Rothberg, K.G., Ying, Y.S., Kamen, B.A., Anderson, R.G., 1990b. J. Cell Biol. 111, 2931–2938.
Rothberg, K.G., Ying, Y.S., Kolhouse, J.F., Kamen, B.A., Anderson, R.G., 1990a. J. Cell Biol. 110, 637–649.
Sperling, R.A., Gil, P.R., Zhang, F., Zanella, M., Parak, W.J., 2008. Chem. Soc. Rev. 37, 1896–1908.
Stella, B., Arpicco, S., Peracchia, M.T., 2000. J. Pharm. Sci. 89, 1452–1464.
Tang, B., Liu, X., Xu, K.H., Huang, H., Yang, G.W., An, L.G., 2007. Chem. Commun., 3726–3728.
Tsou, C., Hung, Y., Mou, C., 2014. Microporous Mesoporous Mater 190, 181–188.
Turek, J.J., Leamon, C.P., Low, P.S., 1993. J. Cell Sci. 106, 423–430.
Varma, R., Mayor, S., 1998. Nature 394, 798–801.
Wang, H., Zheng, L., Peng, C., Shen, M., Shi, X., Zhang, G., 2013. Biomaterials 34, 470–480.
Webb, B.A., Chimenti, M., Jacobson, M.P., Barber, D.L., 2011. Nat. Rev. Cancer 11, 671–677.
Wei, H., Wang, Z., Yang, L., Tian, S., Hou, C., Lu, Y., 2010. Analyst 135, 1406–1410.
Wu, M., Fan, J., Gunning, W., Ratnam, M., 1997. J. Membr. Biol. 159, 137–147.
Xie, J., Zheng, Y., Ying, J.Y., 2009. J. Am. Chem. Soc. 131, 888–889.
Xue, M., Wang, X., Duan, L., Gao, W., Ji, F., Tang, B., 2012. Biosens. Bioelectron 36, 168–173.
Zhang, X., Lin, Y., Gillies, R.J., 2010. J. Nucl. Med. 51, 1167–1170.
Zhuang, M., Ding, C., Zhu, A., Tian, Y., 2014. Anal. Chem. 86, 1829–1836.
Zhu, A., Qu, Q., Shao, X., Kong, B., Tian, Y., 2012. Angew. Chem. Int. Ed. 51, 7185–7189.